THE JOURNAL OF PHYSICAL CHEMISTRY A
A JOURNAL OF THE AMERICAN CHEMICAL SOCIETY

pubs.acs.org/JPCA

Article

Kinetic and Dynamic Studies of the F(^{2}P) + ND_3 → DF + ND_2 Reaction

Rong Xin, Haipan Xiang, Li Tian, Yong Li,* and Hongwei Song*

Cite This: *J. Phys. Chem. A* 2021, 125, 8025–8032

Read Online

ACCESS | Metrics & More | Article Recommendations

ABSTRACT: The fast F reaction with NH_3 poses a big challenge to experimental studies because of secondary chemical and collisional reactions. The quasi-classical trajectory method is utilized to investigate the mode specificity, product energy disposal, and temperature dependence of the thermal rate coefficient of F + ND_3 → DF + ND_2 on a recently developed potential energy surface. The effect of isotopic substitution is explored by comparing the F + ND_3 reaction with the F + NH_3 reaction. The computed results permit a better understanding of the F + ammonia reaction. The DF vibrational state has a Λ-type distribution, in accordance with the experimental measurement by the fast flow reactor technique. The product ND_2 is dominantly populated in the ground state, and a considerable amount of ND_2 is produced in the fundamental states of the bending mode. The similar vibrational state distributions of HF and NH_2 in the F + NH_3 reaction indicate a weak isotopic substitution effect on the product energy disposal. Exciting the umbrella mode of ND_3 suppresses the reaction at low energies below 5 kcal mol^{-1}, in sharp contrast to the observation in the F + NH_3 reaction. These dynamical behaviors can be partially explained by the sudden vector projection model. In addition, the thermal rate coefficient of F + ND_3 shows no temperature dependence in the range between 150 and 2000 K. There exists an inverse kinetic isotope effect at temperatures from 150 to 1500 K.

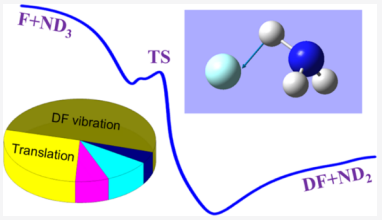

1. INTRODUCTION

The hydrogen abstraction reaction of F with NH_3 takes place very fast and is followed by the secondary reaction of F and NH_2.[1−6] The fast vibrational relaxation via gas-phase collisions and secondary reactions poses a big challenge to the experimental measurement of rovibrational distributions of nascent product HF in the F + NH_3 reaction and DF in the isotopically substituted reaction F + ND_3. The arrested relaxation (AR) technique[1,2,4] and the fast flow reactor (FR) technique[3,6] were utilized to measure product state distributions by observing HF and DF infrared chemiluminescence. Some efforts have also been made toward eliminating vibrational relaxation and secondary reactions in both experiments. The best HF distribution $P(v = 1):P(v = 2)$ was assigned as 57 ± 02:43 ± 02 by the FR,[6] in accordance with 60:40 by AR.[5] In contrast, the DF distribution $P(v = 1):P(v = 2):P(v = 3)$ was determined by AR to be 36:27:37,[4] inconsistent with the distribution of 26.5 ± 1.5:40.0 ± 1.5:33.5 ± 1.5 by the FR.[6] The discrepancy was attributed by Sloan and co-workers to the contribution from the secondary reaction in the AR study.[5] The crossed beam technique was employed by Xiao et al. to measure the product angular distribution and product kinetic energy distribution in the reactions of F with NH_3 and ND_3 with the collision energy of 4.5 kcal mol^{-1}.[7] They found that the products HF and DF are largely forward-scattered relative to the F-atom beam direction, but some sideways and backward scattering exists.

Theoretically, Espinosa-García and Corchado reported a full-dimensional analytical potential energy surface (PES) for the F + NH_3 → HF + NH_2 reaction, denoted as PES-1997 in this work, which was calibrated by the reactant and product properties from experiments and the calculated properties of a hydrogen-bonded complex linking NH_2·HF.[8] Quasi-classical trajectory (QCT) calculations on the analytical PES showed that the differential cross-sections (DCSs) reproduce reasonably well the experimental results, while the agreement between theoretical and experimental product energy partitions was poorer.[9] The disagreement was explained by the excessively attractive interaction from the PES. Recently, we developed an *ab initio*-based PES by fitting 41,282 energy points at the level of UCCSD(T)-F12/aug-cc-pVTZ using the fundamental invariant neural network method (FI-NN),[10,11] denoted as the FI-NN PES.[12] The calculated DCSs and product energy partitions for the F + NH_3 → HF + NH_2 reaction by the QCT method agreed well with the experimental results, verifying the reliability of the PES. Then, the PES was used to predict the reactant mode specificity by carrying out QCT and quantum dynamics simulations.[13] It was found that exciting the low-frequency umbrella mode of NH_3 promotes the reaction much more than exciting the high-frequency stretching modes over a wide range of collision energies.

Received: July 22, 2021
Revised: August 22, 2021
Published: September 3, 2021

https://doi.org/10.1021/acs.jpca.1c06515
J. Phys. Chem. A 2021, 125, 8025–8032

In this work, QCT calculations are carried out on the FI-NN PES to study the mode specificity, product energy partition, vibrational distribution, and temperature dependence of the thermal rate coefficients in the F + ND_3 → HF + ND_2 reaction and the effect of isotopic substitution. The paper is organized as follows. Section 2 outlines the QCT method. The results are provided and discussed in Section 3. Section 4 summarizes the main conclusions of this paper.

2. THEORY

The QCT calculations are implemented by interfacing the FI-NN PES with the modified software VENUS 96.[14] The integral cross-section (ICS) of the reaction is expressed as

$$\sigma_r(E_c) = \pi b_{max}{}^2 P_r(E_c) \quad (1)$$

where the reaction probability $P_r(E_c)$ is defined as the ratio between the number of reactive trajectories N_r and the number of total trajectories N_{tot} at a specific collision energy E_c. The maximum impact parameter, b_{max}, is determined by small batches of trajectories with trial values at each specified initial state and collision energy. The relative statistical error is defined as $\Delta = \sqrt{(N_{tot} - N_r)/N_{tot}N_r}$.

The DCS is obtained by

$$\frac{d\sigma_r}{d\Omega} = \frac{\sigma_r P_r(\theta)}{2\pi \sin(\theta)} \quad (2)$$

where $P_r(\theta)$ is the normalized probability at a scattering angle of θ. The scattering angle θ is given by

$$\theta = \cos^{-1}\left(\frac{\vec{v}_i \cdot \vec{v}_f}{|\vec{v}_i||\vec{v}_f|}\right) \quad (3)$$

in which $\vec{v}_i = \vec{v}_F - \vec{v}_{ND3}$ and $\vec{v}_f = \vec{v}_{DF} - \vec{v}_{ND2}$. In practice, the DCS is calculated by the binning method, for which the trajectory with the scattering angle located within the range of $\theta' \pm 4.5°$ is attributed to θ', where θ' = 4.5, 13.5, ..., 175.5°. $P_r(\theta')$ is calculated by

$$P_r(\theta') = \frac{\sum_{\theta \geq \theta' - 4.5}^{\theta < \theta' + 4.5} N_r(\theta)}{N_r} \quad (4)$$

The rate coefficient at temperature T is calculated by

$$k(T) = \frac{1}{Q_e}\left(\frac{8k_BT}{\pi\mu}\right)^{1/2} \pi b_{max}{}^2 \frac{N_r}{N_{tot}} \quad (5)$$

in which μ is the reduced mass between reactants F and ND_3 and k_B is the Boltzmann constant. Since the spin−orbit splitting of F is taken as 404 cm^{-1},[15] the electronic partition function Q_e is expressed as $(4 + 2e^{-404/k_BT})/2$. At each temperature T, the collision energy and the initial rovibrational energies of ND_3 are sampled according to the Boltzmann distribution.

The vibrational state of the product DF is computed by the Einstein−Brillouin−Keller semiclassical quantization of the action integral.[16] The vibrational state distribution of ND_2 is calculated by the normal mode analysis (NMA) method.[17−20] The coordinates and momenta used in NMA calculations are extracted from a specific step of each trajectory, which is determined on the condition that the corresponding geometry has the lowest potential energy within the last several vibrational periods of ND_2, minimizing the effect of the harmonic approximation.[21−23] Two binning methods, namely, histogram binning (HB)[24] and energy-based Gaussian binning (1GB),[20,25,26] are utilized to assign the product quantum state. The zero-point energy (ZPE) leakage is an intrinsic defect in classical trajectory simulations. The statistics is sometimes seriously disturbed if one discards the trajectories which do not satisfy the ZPE constraint. In this work, a "hard" ZPE constrain is implemented when calculating the product energy disposal, where we discard the trajectories for which either of the products has a vibrational energy lower than its harmonic ZPE.

The reactant ND_3 (NH_3) is initiated from the ground and fundamental states of its normal modes with the collisional energy up to 30 kcal mol^{-1}. When compared with the experimental measurement, the collision energy and rovibrational states are sampled at 300 K. The trajectories are launched from a reactant separation of 8.0 Å and terminated when products or reactants reach a separation of 8.0 Å for reactive or nonreactive trajectories. In the modified software, the reactive or nonreactive event will be checked only if the separation between the two approaching reactants is first smaller than 8.0 Å. The time step is taken as 0.01 fs, which conserves the energy better than 10^{-4} kcal mol^{-1} in the propagation. 80,000−200,000 trajectories are launched from each initial state, which keeps the relative statistical errors all below 1%.

3. RESULTS AND DISCUSSION

Figure 1 shows the schematic diagram of the reaction path on the FI-NN PES. The reaction takes place by overcoming a

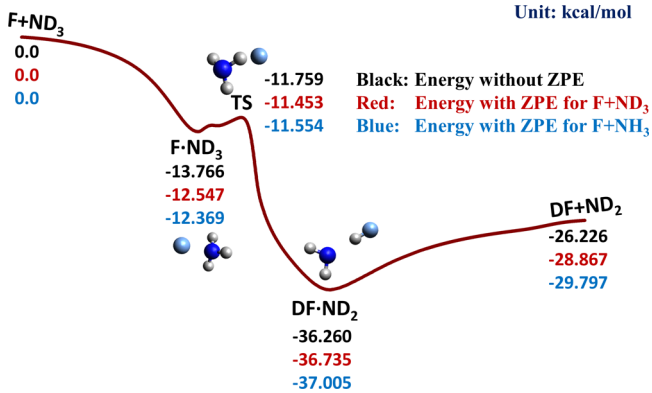

Figure 1. Schematic diagram of the reaction path for the F + ND_3 → DF + ND_2 reaction. The energies of stationary points on the PES (black) and the ZPE-corrected values for the D-abstraction reaction (red) and for the H-abstraction reaction (blue) are shown in proximity to the corresponding geometries.

submerged transition state in between pre- and post-reaction wells. The ZPE-corrected energies of stationary points for the D-abstraction and H-abstraction reactions are given in the figure as well. The calculated ICSs of the F + ND_3 → DF + ND_2 reaction from the ground and fundamental states of ND_3 are shown in the upper panel of Figure 2 as a function of collision energy. The four numbers ν_1, ν_2, ν_3, and ν_4 in the parentheses denote excitations of reactant ND_3 in the symmetric stretching, umbrella, asymmetric stretching, and asymmetric bending modes, respectively. Since this reaction has no activation barrier, the ICS from each state, as expected, declines monotonically with the increase in collision energy. Fundamental excitation of each vibrational mode of ND_3

https://doi.org/10.1021/acs.jpca.1c06515
J. Phys. Chem. A 2021, 125, 8025−8032

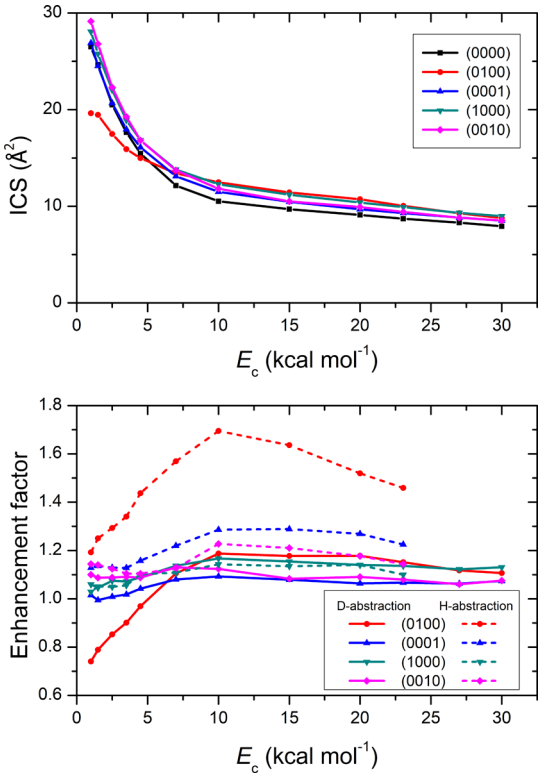

Figure 2. ICSs of the F + ND_3 → DF + ND_2 reaction from the ground and fundamental states of ND_3 vibrational modes in the upper panel and comparison of the enhancement factors between the F + ND_3 and F + NH_3 reactions for the reactant vibrational excitations in the lower panel.

promotes the reaction over the energy range studied except for the umbrella mode. Exciting the umbrella mode enhances the reaction at collision energies above about 5 kcal mol^{-1}, while it inhibits the reaction at lower energies. This is in sharp contrast to the observation in the F + NH_3 → HF + NH_2 reaction, in which the umbrella mode has the highest efficacy in promoting the reaction at collision energies from 1 to 23 kcal mol^{-1}.[13] The lower panel presents the enhancement factor for exciting each vibrational mode of ND_3, together with the result for the F + NH_3 reaction.[12] The enhancement effect for the reactant vibrational excitation is stronger in the H-abstraction reaction than that in the D-abstraction reaction except for the symmetric stretching mode. Exciting the symmetric stretching modes of ND_3 and NH_3 gives a similar enhancement effect on the corresponding reaction. As expected, the largest discrepancy occurs for the umbrella mode, and the enhancement factor in the H-abstraction reaction is about 1.5 times larger than that in the D-abstraction reaction. However, it is noted that the ups and downs of the enhancement factor with the translational energy in the D-abstraction reaction match the changes in the H-abstraction reaction, implying that both reactions take place in the same mechanism.

To clarify the underlying reaction mechanisms, the DCSs from different initial states are depicted in Figure 3 with the collision energy fixed at 4.5, 10.0, 20.0, and 30.0 kcal mol^{-1}. Clearly, the reaction is dominated by forward scattering, and sideways and backward scatterings have noticeable contributions at low collision energies. When the umbrella mode is excited, forward and backward scatterings are suppressed compared with the corresponding ground-state DCS at E_c = 4.5 kcal mol^{-1}. As the collision energy increases, forward scattering is apparently enhanced by exciting the umbrella mode, although backward scattering is slightly prohibited. In contrast, excitation of all the other modes of ND_3 enhances forward scattering and yet has a negligible effect on backward scattering.

In the F + NH_3 → HF + NH_2 reaction, forward scattering is, however, significantly enhanced by exciting the umbrella mode of NH_3 at both low and high collision energies.[13] QCT calculations are also carried out by replacing the hydrogen atom in NH_3 with tritium. The reactivity is suppressed at low collision energies as well. Compared with the ground-state reaction, the direct stripping mechanism is more favored by exciting the reactant umbrella mode in the hydrogen transfer reaction, while it becomes less favored in the deuterium transfer reaction.

The product energy partitioning for the F + ND_3 → DF + ND_2 reaction at T = 300 K is plotted in the upper panel of Figure 4, together with the available experimental[2,6] and theoretical results[9] for comparison. f_v, f_{trans}, and f_r in the figure represent the fractions of the released energy in the product vibration, translation, and rotation, respectively. The average available energy at T = 300 K is 30.60 kcal mol^{-1}. The ZPEs are removed from the vibrational energies of the products DF and ND_2. The QCT calculations show that 51% of the available energy is released as the vibrational energy of DF, followed by the translational energy with a proportion of 28%, and the ND_2 vibration accounts for 10%. A relatively small account of energy flows into the rotational modes of DF and ND_2, implying that the rotational motions of DF and ND_2 are loosely coupled with the reaction coordinate. By analyzing the geometry change along the minimum energy path, the bond distance of HF, in the same way as that for DF, is shortened from 1.5 to 0.918 Å from the transition state (TS)to the products, respectively, and the bending angle of D−N−D varies from 112.34 to 103.03°. Therefore, the significant geometry changes from the TS to the products facilitate the energy to flow into the corresponding product vibrational modes. On the other hand, as mentioned above, the reaction is dominated by the direct stripping mechanism, which favors the energy to be released as the product translational energy.

This theoretical product energy partitioning agrees well with the experimental measurements[2,6] for the vibration and rotation of the product DF. In contrast, Espinosa-García and Monge-Palacios's QCT calculations on the PES-1997 overestimated the proportion of the rotational energy of DF.[9] The overestimation was attributed to an excessively attractive character of the stretching terms of the function form in building the PES-1997. In addition, the collision energy was fixed at E_c = 4.5 kcal mol^{-1} in their work, different from the experimental condition.

To explore isotopic substitution effects, the product energy partitioning for the F + NH_3 → HF + NH_2 reaction at T = 300 K is calculated as well and depicted in the lower panel of Figure 4. The average available energy is 31.57 kcal mol^{-1}. The vibrational energy of HF accounts for 45% of the available energy. The translational energy has a proportion of 31%, and the NH_2 vibration contributes 11%. The rest flows into the rotational modes of HF and NH_2. The theoretical energy disposal reproduces reasonably well available experimental results.[2,6] The fraction of vibrational energy released to HF (45%) is 6% less than that released to DF (51%), in good agreement with Wategaonkar and Setser's experimental value

https://doi.org/10.1021/acs.jpca.1c06515
J. Phys. Chem. A 2021, 125, 8025−8032

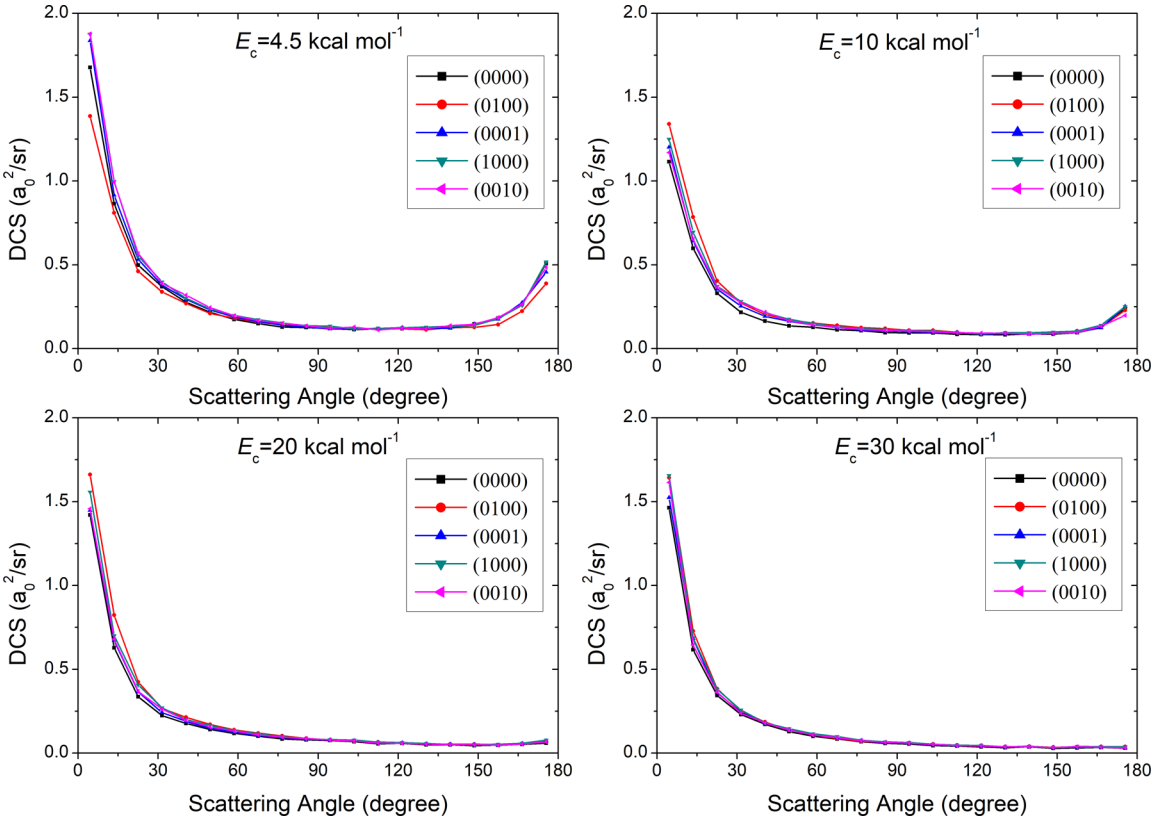

Figure 3. DCSs from the ground and fundamental states of ND_3 vibrational modes with the collision energy E_c fixed at 4.5, 10.0, 20.0, and 30.0 kcal mol^{-1}.

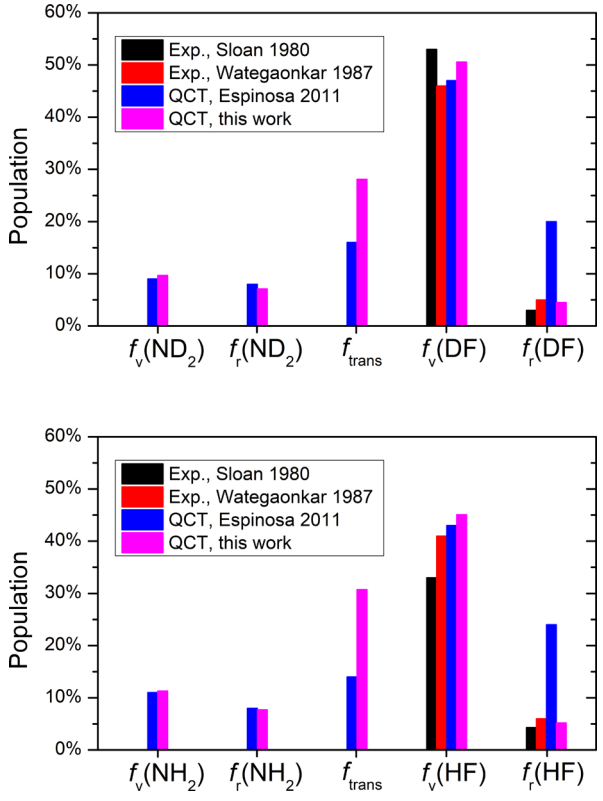

Figure 4. Comparison of product energy disposals for the F + ND_3 and F + NH_3 reactions at T = 300 K.

of 5% from 41 to 46%.[6] The slightly lower value of f_v(HF) than that for many H-abstraction reactions was attributed by Wategaonkar and Setser to attractive (H-bonding interactions) secondary encounters between HF and NH_2 in the exit channel. This is also supported by the QCT calculations, in which the colliders undergo several collisions before separating into products for indirect trajectories.

The product DF in the F + ND_3 reaction was observed by AR to yield a noninverted vibrational distribution for $P(\nu = 1)$:$P(\nu = 2)$,[4] in sharp contrast to the FR measurement that gave an inverted distribution.[6] In order to provide a theoretical prediction, the vibrational state distributions of the products DF and ND_2 are calculated on the FI-NN PES as well, as shown in the upper panels of Figure 5 and 6, respectively. Since the two binning methods, HB and GB, give similar vibrational state distributions for both DF and ND_2, the following discussions are based on the GB results. In the upper panel of Figure 4, the vibrational state distribution of DF follows the order of $P(\nu = 0) < P(\nu = 1) < P(\nu = 2) > P(\nu = 3) > P(\nu = 4)$; that is, it first increases with the increasing vibrational excitation for $\nu \leq 2$ and then starts to decline. The available experimental and theoretical results are presented in the same figure as well for comparison. Note that it is impossible to directly determine the $\nu = 0$ population due to experimental limitations. Donaldson et al.'s experimental results[4] show a V-type distribution for $\nu = 1-3$, inconsistent with our theoretical results. When comparing the theoretical results with Wategaonkar and Setser's experimental results,[6] Setser suggests using the results in which the $\nu = 0$ population was assigned assuming a linear surprisal plot (three-body prior). It can be seen that our theoretical distribution, no

https://doi.org/10.1021/acs.jpca.1c06515
J. Phys. Chem. A 2021, 125, 8025−8032

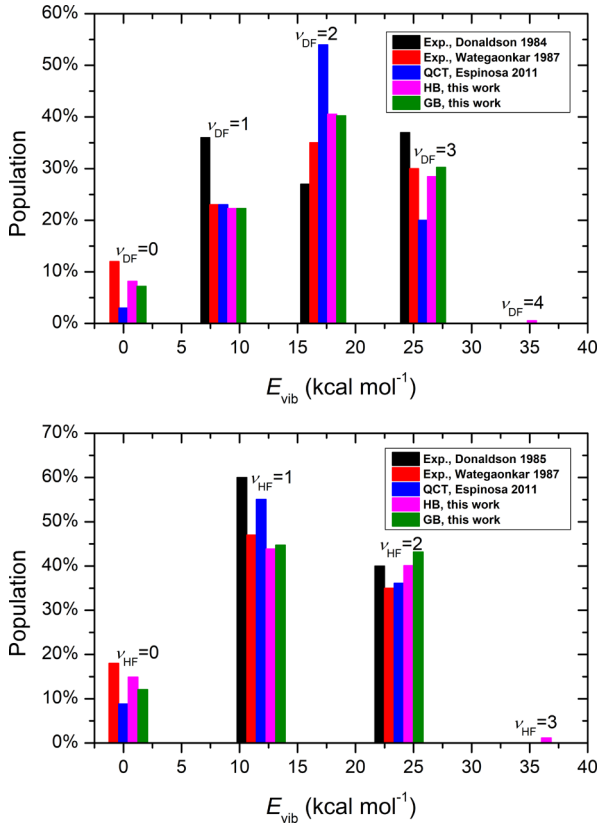

Figure 5. Comparison of vibrational state distributions between DF and HF for the F + ND_3 and F + NH_3 reactions at T = 300 K.

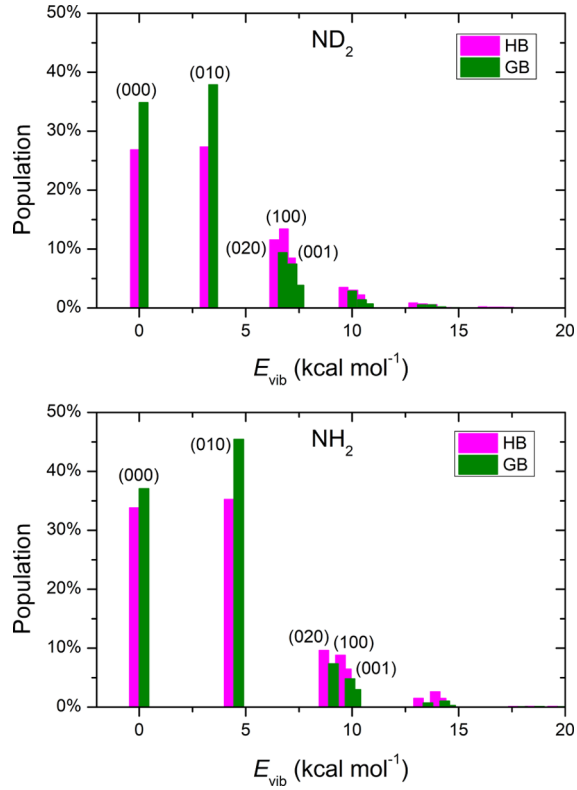

Figure 6. Comparison of vibrational state distributions between ND_2 and NH_2 for the F + ND_3 and F + NH_3 reactions at T = 300 K.

matter the trend and the amplitude, agrees well with their experimental measurement. In addition, Espinosa's theoretical distribution is in reasonable agreement with Wategaonkar and Setser's experimental distribution,[6] yet the population of $\nu = 2$ is significantly overestimated.[9]

The vibrational state distribution of HF is given in the lower panel of Figure 5 for comparison. The distribution follows the order of $P(\nu = 0) < P(\nu = 1) \approx P(\nu = 2) > P(\nu = 3)$. In contrast, both experiments showed that the vibrational state of HF has the maximum distribution in the first excited state. It appears that Espinosa's theoretical calculation predicts a consistent peak distribution with the experimental results. Compared with HF, the product DF is more populated in the higher excited states due to the smaller energy level gaps.

Unlike the product DF, ND_2 has a "cold" vibrational distribution. As shown in the upper panel of Figure 6, the product ND_2 is mainly populated in the ground state and the fundamental state of the bending mode, with proportions of 34 and 37%, respectively. The population for each of the other higher excited states is exclusively less than 10%. The lower panel shows the vibrational distribution of NH_2. 37% of NH_2 is populated in the ground state. The fundamental state of the bending mode accounts for 45%, with the other higher excited states having less than 10%. Both distributions indicate that the bending motion is more strongly coupled with the reaction coordinate.

The sudden vector projection (SVP) model has been widely applied to predict the reactant-mode specificity and product energy disposal.[27−40] In the SVP model, the efficacy of a reactant mode in promoting the reaction or the ability of a product mode in gaining the energy released by the reaction is semiquantitatively determined by the projection of the reactant or product-mode vector ($\bar{Q}_i$) onto the reaction coordinate vector ($\bar{Q}_{RC}$) at the transition state: $P_i = \bar{Q}_i \cdot \bar{Q}_{RC} \in [0,1]$.[28,41] In this reaction, the submerged barrier is expected to play a significant role in the direct trajectories. The observed mode specificity and energy disposal are hopefully rationalized, at least partially, by the SVP model. The calculated SVP values are listed in Table 1. For the reactant mode, the umbrella mode has the largest projection of 0.314, followed by the asymmetric stretching mode with 0.137 and the symmetric stretching mode with 0.121. The asymmetric bending mode and the translational mode have negligible coupling with the reaction coordinate. The enhancement effects of exciting the symmetric and asymmetric stretching modes on the reaction agree with the SVP predictions. In contrast, the collision energy dependence of the promotional efficacy of the umbrella cannot be predicted by the SVP model. As for the product mode, the vibrational motion of DF has the largest projection of 0.875, followed by the translational mode with 0.341 and the bending mode with 0.102. These projections predict that the DF vibration will be highly excited in the reaction. A large amount of energy will also flow into the product translational

Table 1. SVP Values for the F + ND_3 (ν_1,ν_2,ν_3,ν_4) → DF (ν_{DF}) + ND_2 (ν'_1,ν'_2,ν'_3) Reaction

reactant mode	SVP	product mode	SVP
ν_1 (symmetric stretch)	0.121	ν_{DF}	0.875
ν_2 (umbrella)	0.314	ν'_1 (symmetric stretch)	0.020
ν_3 (asymmetric stretch)	0.137	ν'_2 (bend)	0.102
ν_4 (asymmetric bend)	0.038	ν'_3 (asymmetric stretch)	0.000
translational	0.022	translational	0.341

https://doi.org/10.1021/acs.jpca.1c06515
J. Phys. Chem. A 2021, 125, 8025−8032

mode, and a fraction of the energy goes into the bending mode of ND_2. These predictions are well consistent with the QCT calculations. Therefore, the product energy disposal can be rationalized, at least to some extent, by the coupling between the product normal-mode vector and the reaction coordinate at the transition state.

The thermal rate coefficients of the F + NH_3 → HF + NH_2 reaction was reported by Persky[42,43] and Walther and Wagner to have different temperature dependencies at 270−330 K. In contrast, theoretical calculations showed practically no temperature dependence within the statistical errors. In this work, the thermal rate coefficients of the F + ND_3 → DF + ND_2 reaction are calculated on the FI-NN PES. The upper panel of Figure 7

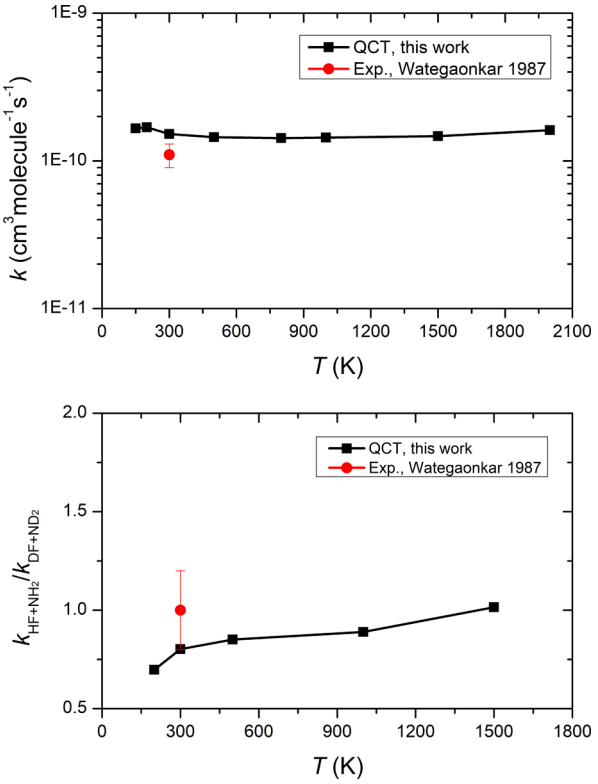

Figure 7. Comparison of calculated and measured thermal rate constants for the F + ND_3 → DF + ND_2 reaction (upper panel) and the KIE (lower panel).

compares the calculated thermal rate coefficients with the available experimental result.[3] The corresponding values are listed in Table 2. Similar to that of the F + NH_3 → HF + NH_2 reaction, the rate coefficient is nearly unchanged in the temperature range from 150 to 2000 K, implying no temperature dependence. The rate coefficient was measured by Wategaonkar and Setser to be 1.1 ± 0.2 × 10^{-10} cm^3 $molecule^{-1}$ s^{-1} at 300 K,[6] close to the theoretical value of 1.52 × 10^{-10} cm^3 $molecule^{-1}$ s^{-1}. The lower panel compares the calculated kinetic isotope effect (KIE) with Wategaonkar and Setser's experimental results.[6] The QCT calculation predicts an inverse KIE at temperatures below 1500 K, and the KIE becomes weaker as the temperature increases. In sharp contrast, the experimental measurement gave a vanishing KIE at T = 300 K. The inverse KIE seems to be unusual for an abstraction reaction. However, as mentioned above, the indirect mechanism plays a significant role in the reaction at low temperature (collision energy) due to the existence of wells in the entrance and exit channels, which possibly results in a different KIE from that in direct abstraction reactions. In fact, the experiment cannot exclude the existence of an inverse KIE in the reaction due to its errors. On the other hand, the quantum effects, such as tunneling and resonance, in the H-abstraction reaction is believed to be stronger than those in the D-abstraction reaction. These effects are completely neglected in the QCT method due to its inherent drawback, which brings some uncertainty for the theoretical results. If included, the theoretical ratio should increase and possibly match the experimental value.

Table 2. Thermal Rate Coefficients (×10^{-10} cm^3 $molecule^{-1}$ s^{-1}) for the F + ND_3 → DF + ND_2 Reaction

T (K)	QCT[a]	exp.[b]
150	1.66	1.1 ± 0.2
200	1.69	
300	1.52	
500	1.45	
800	1.43	
1000	1.44	
1500	1.47	
2000	1.61	

[a]this work. [b]ref 6.

4. CONCLUSIONS

In this work, the QCT method is employed to investigate the dynamics and kinetics of the F + ND_3 → DF + ND_2 reaction and the effect of isotopic substitution. On one hand, exciting the umbrella mode of ND_3 promotes the reaction at a high collision energy and yet inhibits the reaction at a relatively low energy. This is different from what we have observed in the F + NH_3 → HF + NH_2 reaction, where exciting the umbrella mode of NH_3 significantly enhances the reaction over the energy range studied. The direct stripping mechanism is more favored by exciting the reactant umbrella mode in the hydrogen transfer reaction while becoming less favored in the deuterium transfer reaction.

The calculated product energy partition agrees well with the experimental measurement at T = 300 K. 51% of the available energy flows into the DF vibrational mode, followed by the translational energy with a proportion of 28% and the ND_2 vibration with 10%. The vibrational state of DF has a Λ-type distribution; the population first increases and then declines with the increasing vibrational excitation. The vibrational distribution is consistent with Wategaonkar and Setser's experimental result. The product ND_2 shows a "cold" vibrational distribution, which is mainly populated in the ground state and the fundamental state of the bending mode. These dynamic behaviors can be partially rationalized by the coupling of the product vibrational motion with the reaction coordinate at the transition state. The vibrational state distributions of HF and NH_2 in the F + NH_3 reaction are slightly different from that observed in the F + ND_3 reaction. In addition, the thermal rate coefficient of the F + ND_3 → DF + ND_2 reaction has no temperature dependence within the statistical errors. There exists an inverse KIE at temperatures ranging from 150 to 1500 K.

https://doi.org/10.1021/acs.jpca.1c06515
J. Phys. Chem. A 2021, 125, 8025−8032

AUTHOR INFORMATION

Corresponding Authors

Yong Li − *College of Physical Science and Technology, Huazhong Normal University, Wuhan 430079, China*; Email: yongli@mail.ccnu.edu.cn

Hongwei Song − *State Key Laboratory of Magnetic Resonance and Atomic and Molecular Physics, Innovation Academy for Precision Measurement Science and Technology, Chinese Academy of Sciences, Wuhan 430071, China*; orcid.org/0000-0001-8401-2364; Email: hwsong@wipm.ac.cn

Authors

Rong Xin − *State Key Laboratory of Magnetic Resonance and Atomic and Molecular Physics, Innovation Academy for Precision Measurement Science and Technology, Chinese Academy of Sciences, Wuhan 430071, China; College of Physical Science and Technology, Huazhong Normal University, Wuhan 430079, China*

Haipan Xiang − *State Key Laboratory of Magnetic Resonance and Atomic and Molecular Physics, Innovation Academy for Precision Measurement Science and Technology, Chinese Academy of Sciences, Wuhan 430071, China; College of Physical Science and Technology, Huazhong Normal University, Wuhan 430079, China*

Li Tian − *State Key Laboratory of Magnetic Resonance and Atomic and Molecular Physics, Innovation Academy for Precision Measurement Science and Technology, Chinese Academy of Sciences, Wuhan 430071, China; College of Physical Science and Technology, Huazhong Normal University, Wuhan 430079, China*

Complete contact information is available at: https://pubs.acs.org/10.1021/acs.jpca.1c06515

Notes

The authors declare no competing financial interest.

ACKNOWLEDGMENTS

We would like to thank Prof. D. W. Setser from Kansas State University for reading through the draft and insightful suggestions. This work is supported by the National Natural Science Foundation of China under grant no. 21973109.

REFERENCES

(1) Douglas, D. J.; Sloan, J. J. The dynamics of the reactions of fluorine atoms with ammonia and hydrazine. *Chem. Phys.* **1980**, *46*, 307−312.

(2) Slaon, J. J.; Watson, D. G.; Williamson, J. The detailed isotope effect in the F + NH_3 and F + ND_3 reactions. *Chem. Phys. Lett.* **1980**, *74*, 481−485.

(3) Manocha, A. S.; Setser, D. W.; Wickramaaratchi, M. A. Vibrational energy disposal in reactions of fluorine atoms with hydrides of groups III, IV and V. *Chem. Phys.* **1983**, *76*, 129−146.

(4) Donaldson, D. J.; Parsons, J.; Sloan, J. J.; Stolow, A. Vibrational energy partitioning in the reaction of F atoms with NH_3 and ND_3. *Chem. Phys.* **1984**, *85*, 47−62.

(5) Donaldson, D. J.; Sloan, J. J.; Goddard, J. D. Energy partitioning in atom−radical reactions: The reaction of F atoms with NH_2. *J. Chem. Phys.* **1985**, *82*, 4524−4536.

(6) Wategaonkar, S.; Setser, D. W. Vibrational energy disposal in the reactions of F atoms with NH_3, ND_3, N_2H_4, and CH_3ND_2. *J. Chem. Phys.* **1987**, *86*, 4477−4487.

(7) Xiao, C.; Shen, G.; Wang, X.; Fan, H.; Yang, X. Crossed Beams Study on the Dynamics of the F-Atom Reaction with Ammonia. *J. Phys. Chem. A* **2010**, *114*, 4520−4523.

(8) Espinosa-García, J.; Corchado, J. C. Analytical Surface for the Reaction with No Saddle-Point NH_3 + F → NH_2 + FH. Application of Variational Transition State Theory. *J. Phys. Chem. A* **1997**, *101*, 7336−7344.

(9) Espinosa-García, J.; Monge-Palacios, M. Theoretical Study of the F + NH_3 and F + ND_3 Reactions: Mechanism and Comparison with Experiment. *J. Phys. Chem. A* **2011**, *115*, 13759−13763.

(10) Shao, K.; Chen, J.; Zhao, Z.; Zhang, D. H. Communication: Fitting potential energy surfaces with fundamental invariant neural network. *J. Chem. Phys.* **2016**, *145*, 071101.

(11) Chen, R.; Shao, K.; Fu, B.; Zhang, D. H. Fitting Potential Energy Surfaces with Fundamental Invariant Neural Network. II. Generating Fundamental Invariants for Molecular Systems with up to Ten Atoms. *J. Chem. Phys.* **2020**, *152*, 204307.

(12) Tian, L.; Zhu, Y.; Song, H.; Yang, M. Theoretical study of the F(^{2}P) + NH_3 → HF + NH_2 reaction on an accurate potential energy surface: dynamics and kinetics. *Phys. Chem. Chem. Phys.* **2019**, *21*, 11385−11394.

(13) Tian, L.; Song, H.; Yang, M. Effects of bending excitation on the reaction dynamics of fluorine atoms with ammonia. *Phys. Chem. Chem. Phys.* **2021**, *23*, 2715−2722.

(14) Hase, W. L.; Duchovic, R. J.; Hu, X.; Komornicki, A.; Lim, K. F.; Lu, D.-H.; Peslherbe, G. H.; Swamy, K. N.; Vande Linde, S. R.; Varandas, A.; et al. VENUS96: A general chemical dynamics computer program. *Quantum Chem Program Exch Bull* **1996**, *16*, 43.

(15) Nguyen, T. L.; Li, J.; Dawes, R.; Stanton, J. F.; Guo, H. Accurate Determination of Barrier Height and Kinetics for the F + H_2O → HF + OH Reaction. *J. Phys. Chem. A* **2013**, *117*, 8864−8872.

(16) Gutzwiller, M. C. *Chaos in Classical and Quantum Mechanics*; Springer: New York, 1990.

(17) Espinosa-García, J.; Bravo, J. L.; Rangel, C. New Analytical Potential Energy Surface for the F(^{2}P) + CH_4 Hydrogen Abstraction Reaction: Kinetics and Dynamics. *J. Phys. Chem. A* **2007**, *111*, 2761−2771.

(18) Espinosa-García, J.; Bravo, J. L. State-to-State Dynamics Analysis of the F + CHD_3 Reaction: A Quasiclassical Trajectory Study. *J. Phys. Chem. A* **2008**, *112*, 6059−6065.

(19) Corchado, J. C.; Espinosa-Garcia, J. Product Vibrational Distributions in Polyatomic Species Based on Quasiclassical Trajectory Calculations. *Phys. Chem. Chem. Phys.* **2009**, *11*, 10157−10164.

(20) Czakó, G.; Bowman, J. M. Quasiclassical Trajectory Calculations of Correlated Product Distributions for the F +CHD_3(v_1=0,1) Reactions Using an Ab Initio Potential Energy Surface. *J. Chem. Phys.* **2009**, *131*, 244302.

(21) Ping, L.; Tian, L.; Song, H.; Yang, M. New Method To Extract Final-State Information of Polyatomic Reactions Based on Normal Mode Analysis. *J. Phys. Chem. A* **2018**, *122*, 6997−7005.

(22) Ping, L.; Zhu, Y.; Li, A.; Song, H.; Li, Y.; Yang, M. Dynamics and kinetics of the reaction OH + H_2S → H_2O + SH on an accurate potential energy surface. *Phys. Chem. Chem. Phys.* **2018**, *20*, 26315−26324.

(23) Zhu, Y.; Ping, L.; Bai, M.; Liu, Y.; Song, H.; Li, J.; Yang, M. Tracking the Energy Flow in the Hydrogen Exchange Reaction OH + H_2O → H_2O + OH. *Phys. Chem. Chem. Phys.* **2018**, *20*, 12543−12556.

(24) Truhlar, D. G.; Muckerman, J. T. Reactive Scattering Cross Sections III: Quasiclassical and Semiclassical Methods. In *Atom-Molecule Collision Theory*; Bernstein, R. B., Ed.; Plenum Press: New York, 1979; pp 505−566.

(25) Bonnet, L.; Rayez, J.-C. Gaussian weighting in the quasiclassical trajectory method. *Chem. Phys. Lett.* **2004**, *397*, 106−109.

(26) Bonnet, L.; Espinosa-García, J. The Method of Gaussian Weighted Trajectories. V. On the 1GB Procedure for Polyatomic Processes. *J. Chem. Phys.* **2010**, *133*, 164108.

(27) Jiang, B.; Guo, H. Control of Mode/Bond Selectivity and Product Energy Disposal by the Transition State: X + H_2O (X = H, F, O(^{3}P), and Cl) Reactions. *J. Am. Chem. Soc.* **2013**, *135*, 15251−15256.

(28) Guo, H.; Jiang, B. The Sudden Vector Projection Model for Reactivity: Mode Specificity and Bond Selectivity Made Simple. *Acc. Chem. Res.* **2014**, *47*, 3679−3685.
(29) Li, J.; Guo, H. Mode specificity and product energy disposal in unimolecular reactions: insights from the sudden vector projection model. *J. Phys. Chem. A* **2014**, *118*, 2419−2425.
(30) Jiang, B.; Guo, H. Mode Specificity, Bond Selectivity, and Product Energy Disposal in X + CH_4/CHD_3 (X=H, F, O(^{3}P), Cl, and OH) Hydrogen Abstraction Reactions: Perspective from Sudden Vector Projection Model. *J. Chin. Chem. Soc.* **2014**, *61*, 847−859.
(31) Song, H.; Guo, H. Mode Specificity in the HCl + OH → Cl + H_2O Reaction: Polanyi's Rules vs Sudden Vector Projection Model. *J. Phys. Chem. A* **2015**, *119*, 826−831.
(32) Song, H.; Guo, H. Vibrational and Rotational Mode Specificity in The Cl + H_2O → HCl + OH Reaction: A Quantum Dynamical Study. *J. Phys. Chem. A* **2015**, *119*, 6188−6194.
(33) Wang, Y.; Song, H.; Szabó, I.; Czakó, G.; Guo, H.; Yang, M. Mode-Specific S_N2 Reaction Dynamics. *J. Phys. Chem. Lett.* **2016**, *7*, 3322−3327.
(34) Xie, C.; Jiang, B.; Yang, M.; Guo, H. State-to-State Mode Specificity in F + CHD_3 → HF/DF + CD_3/CHD_2 Reaction. *J. Phys. Chem. A* **2016**, *120*, 6521−6528.
(35) Zheng, R.; Zhu, Y.; Song, H. Mode-specific quantum dynamics and kinetics of the hydrogen abstraction reaction OH + H_2O → H_2O + OH. *Phys. Chem. Chem. Phys.* **2019**, *21*, 24054−24060.
(36) Xin, R.; Pan, M.; Song, H.; Yang, M. Mode- and Bond-Selected Reaction of H with Local Mode Molecule HDS. *J. Phys. Chem. A* **2020**, *124*, 10162−10170.
(37) Lu, D.; Li, J.; Guo, H. Stereodynamical control of product branching in multi-channel barrierless hydrogen abstraction of CH_3OH by F. *Chem. Sci.* **2019**, *10*, 7994−8001.
(38) Lu, D.; Li, J. Mode specificity of a multi-channel reaction prototype: F+CH_3OH→HF+CH_3O/CH_2OH. *Theor. Chem. Acc.* **2020**, *139*, 157.
(39) Lu, D.; Li, J.; Guo, H. Comprehensive Investigations of the Cl +CH_3OH→HCl+CH_3O/CH_2OH Reaction: Validation of Experiment and Dynamic Insights. *CCS Chem.* **2020**, *2*, 882−894.
(40) Liu, Y.; Song, H.; Xie, D.; Li, J.; Guo, H. Mode Specificity in the OH + HO_2 → H_2O + O_2 Reaction: Enhancement of Reactivity by Exciting a Spectator Mode. *J. Am. Chem. Soc.* **2020**, *142*, 3331−3335.
(41) Jiang, B.; Guo, H. Relative efficacy of vibrational vs. translational excitation in promoting atom-diatom reactivity: Rigorous examination of Polanyi's rules and proposition of sudden vector projection (SVP) model. *J. Chem. Phys.* **2013**, *138*, 234104.
(42) Persky, A. The rate constant of the F+NH_3 reaction: Inverse temperature dependence. *Chem. Phys. Lett.* **2007**, *439*, 3−7.
(43) Walther, C.-D.; Wagner, H. G. Über die Reaktionen von F-Atomen mit H_2O, H_2O_2 und NH_3. *Ber. Bunsen-Ges.* **1983**, *87*, 403−409.

https://doi.org/10.1021/acs.jpca.1c06515
J. Phys. Chem. A 2021, 125, 8025−8032